JOURNAL OF MATERIALS SCIENCE 24 (1989) 3660–3666

Elastic constants of the iron oxide doped yttria-stabilized zirconia

M. A. EWAIDA, A. A. HIGAZY
Physics Department, Faculty of Science, Al-Monoufia University, Shebin Al-Koam, Egypt
B. BRIDGE
Physics Department, Brunel University, Uxbridge, Middlesex, England
M. M. ABOU SEKKINA
Chemistry Department, Faculty of Science, Tanta University, Tanta, Egypt

Ultrasonic compressional and shear wave velocity measurements have been made on the $(ZrO_2)_{1-A}(Y_2O_3)_{A-X}(Fe_2O_3)_X$ system at 5 MHz. The amounts of Fe_2O_3 dopant ranging from 0 up to 10 mol% were mixed with the ceramic matrix. In this paper the ultrasonic compressional and shear wave velocity measurements made on this system at room temperature are discussed. The elastic moduli, Poisson's ratio and density are found to be sensitive to the additions of the Fe_2O_3 dopant and they show an anomalous behaviour. A qualitative explanation of the compositional dependence of the elastic moduli and Poisson's ratio is given in terms of changes in packing density, bond strength, co-ordination number and cross-link density.

1. Introduction

There has recently been considerable interest in the studying of the properties of partially or fully stabilized zirconia [1–21]. Much of this interest arose from using these materials as nozzles for flow-rate control in continuous casting steel, particularly in long-term casting due to their inherent corrosion resistance [17].

Also, considerable progress has been made in developing a ZrO_2-based exhaust-glass sensor to detect the stochiometric air–fuel ratio for closed-loop engine emission control [5, 8, 11]. Wilhelm *et al.* [13] also, have concluded that multivalent transition metal oxide doped ZrO_2 ceramics are useful as self compensating electrolytes for special ZrO_2 oxygen sensors used for the accurate detection of the lean air–fuel ratio in automative engine exhaust gas.

In general, the properties of a ceramic are dependent upon composition, thermal history, microstructure processing and chemical and phase homogeneity. So, with the aim of developing a stabilized zirconia, an ultrasonic study was made on the $(ZrO_2)_{1-A}(Y_2O_3)_{A-X}(Fe_2O_3)_X$ system. From the variation of ultrasonic properties with gradual changes in ceramic composition, information can be obtained about the atomic and molecular configuration in the ceramic.

2. Experimental procedure

2.1. Sample preparation

The ceramics used for the measurements reported here were prepared from laboratory reagent grades of high purity (99.90%) ZrO_2, Y_2O_3 and Fe_2O_3 oxides. The reagents were mixed in a ball mill and mixtures were ground in agate mortar for half an hour; then a few drops of distilled water added as a binder, after which the mixtures were pressed at 3.5 tons for 3 min under vacuum, to yield discs suitable for our measurements. The specimens were heated for 24 h at 110° C to prevent uneven shrinkage warping or cracking. After this treatment, they were fired at different sintering temperatures (1300–1450° C) in a muffle furnace in air for 1 h (in this investigation the specimens fired at 1350 and 1450° C are used). The specimens and furnace were allowed to cool to room temperature.

2.2. Density measurements

The bulk density and true density (specific gravity) of the specimens were determined using Archimedes principle according to the following equation:

$$\text{Bulk density} = \frac{W_S}{W_T}\varrho_T \qquad (1)$$

where W_S denotes the weight of specimen in air, W_T is the apparent weight loss in toluene, and ϱ_T is the density of toluene.

The true density (D) of the specimens was determined using the pycnometer according to the following expression:

$$D = \frac{M_1 - M}{(M_3 - M) - (M_2 - M_1)} \qquad (2)$$

where M is the mass of the empty pycnometer, M_1 denotes the mass of pycnometer with the sample, M_2 is the mass of the pycnometer with sample and water, and M_3 is the mass of the pycnometer filled with water only.

2.3. X-ray diffraction measurements

Extensive X-ray diffraction investigations on the Toronto double doped highly stabilized zirconia refractories have been made [22]. The structure of the fired

0022–2461/89 $03.00 + .12

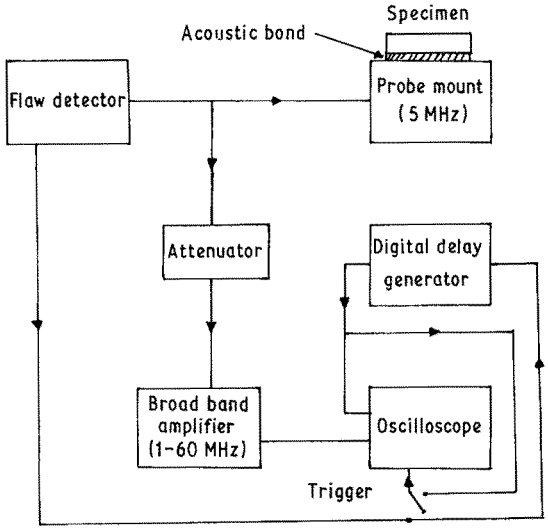

Figure 1 Diagram of the instrumentation of the ultrasonic wave velocity measurements.

specimens was investigated using an X-ray diffractometer type XD-3 (Shimadzu, Japan), with a copper target and nickel filter at a scanning speed $(2\theta) = 2° \text{min}^{-1}$, in the range $2\theta = 20$–$70°$. This range was chosen because it comprises the most intense peaks associated with the crystalline phases.

2.4. Ultrasonic measurements

The method we chose for our work was The Pulse-Echo-Time of Flight Method with time differences between chosen points in an echo train being measured directly on a cathode ray oscilloscope (CRO) screen by means of a high precision digital delay generator. Details of this technique are presented elsewhere [23]. A diagram of the apparatus is shown in Fig. 1. The ultrasonic compressional and shear waves were transmitted and received by commercial transducers (longitudinal transducer 5 MHz, 1.6 cm active diameter; shear-kraut-kramer 4 MHz, 1.3 cm active diameter) actuated by an ultrasonic flaw detector. The output of the transducers was passed through a broad band amplifier (Arenberg 600 E) and displayed, unrectified on a Tektronix 466 100 MHz oscilloscope.

With direct time of flight measurement using a digital delay generator, the absolute velocity can be measured to an accuracy of 0.02%.

The elastic constants of the ceramics were calculated at room temperature from the measured densities and the velocities of longitudinal (V_L) and shear (V_S) ultrasound waves, using the following expressions:

Longitudinal modulus $L = \varrho V_L^2$

Shear modulus $G = \varrho V_S^2$

Bulk modulus $K = L - (4/3)G$

Poisson's ratio $\sigma = (V_L^2 - 2V_S^2)/2(V_L^2 - V_S^2)$

Young's modulus $E = (1 + \sigma)2G$

3. Results and discussion

3.1. X-ray diffraction studies

The X-ray diffraction patterns for the $(ZrO_2)_{0.9}(Y_2O_3)_{0.1}$ specimen fired at various sintering temperatures are shown in Fig. 2. From inspection of this figure, we observed that, on sintering at 1300° C for 1 h, the samples display cubic and monoclinic zirconia solid

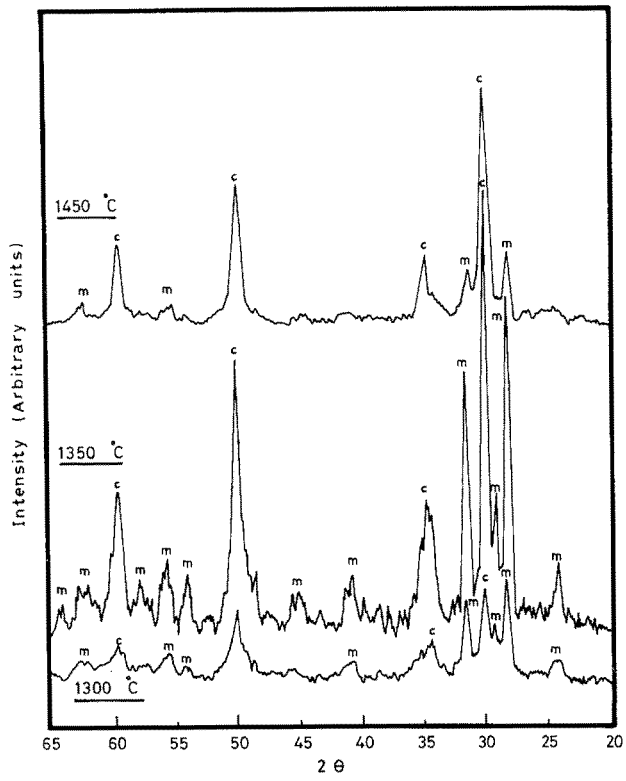

Figure 2 The room temperature Cu$K\alpha$ X-ray diffraction patterns for $(ZrO_2)_{0.9}(Y_2O_3)_{0.1}$ fired at various temperatures. (c = cubic zirconia solid solution; m = monoclinic zirconia solid solution).

solution (SS). As the sintering temperature increases to 1450° C the diffractograms corresponding to cubic zirconia SS grow at the expense of the present monoclinic zirconia phase.

Fig. 3 shows the X-ray diffraction patterns for the $(ZrO_2)_{0.9}(Y_2O_3)_{0.07}(Fe_2O_3)_{0.03}$ specimen fired at different sintering temperatures. It was observed that, at 1300° C sintering, both monoclinic and cubic zirconia

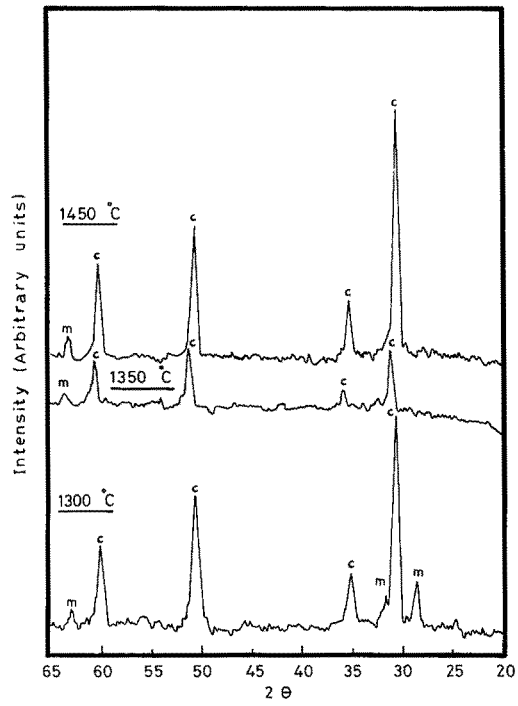

Figure 3 The room temperature Cu$K\alpha$ X-ray diffraction patterns for $(ZrO_2)_{0.9}(Y_2O_3)_{0.07}(Fe_2O_3)_{0.03}$ fired at different temperatures. (c = cubic zirconia solid solution; m = monoclinic zirconia solid solution).

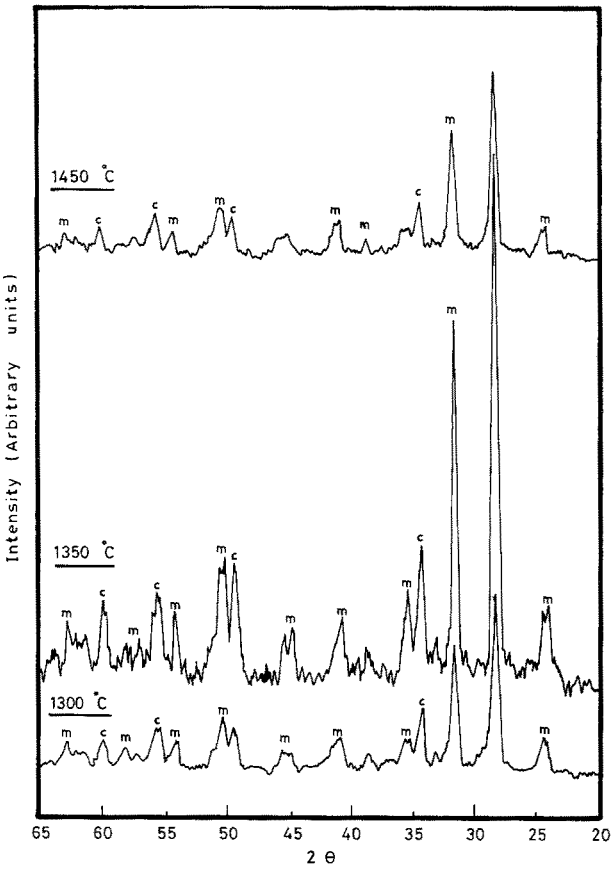

Figure 4 The room temperature Cu$K\alpha$ X-ray diffraction patterns for $(ZrO_2)_{0.9}(Fe_2O_3)_{0.1}$ fired at various temperatures. (c = cubic zirconia solid solution; m = monoclinic zirconia solid solution).

SS are present indicating partial stabilization. As the sintering temperature rises the peaks corresponding to cubic zirconia SS grow, and in the same time the peaks corresponding to monoclinic zirconia weaken. Further increases in sintering temperature cause complete disappearance of monoclinic zirconia, this indicating a complete transformation to cubic zirconia SS.

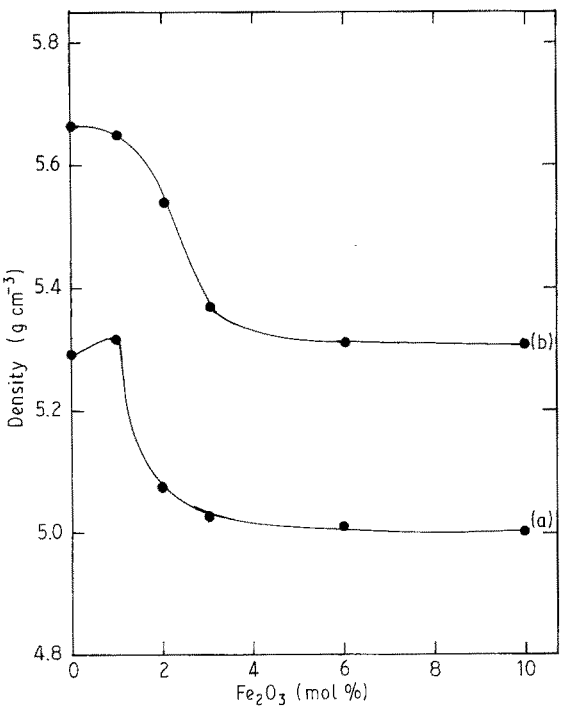

Figure 5 Variation of density with Fe_2O_3 mol % in $(ZrO_2)_{0.9}(Y_2O_3)_{0.1-x}(Fe_2O_3)_x$ ceramic system. (a) and (b) denote specimens fired at 1350 and 1450° C, respectively.

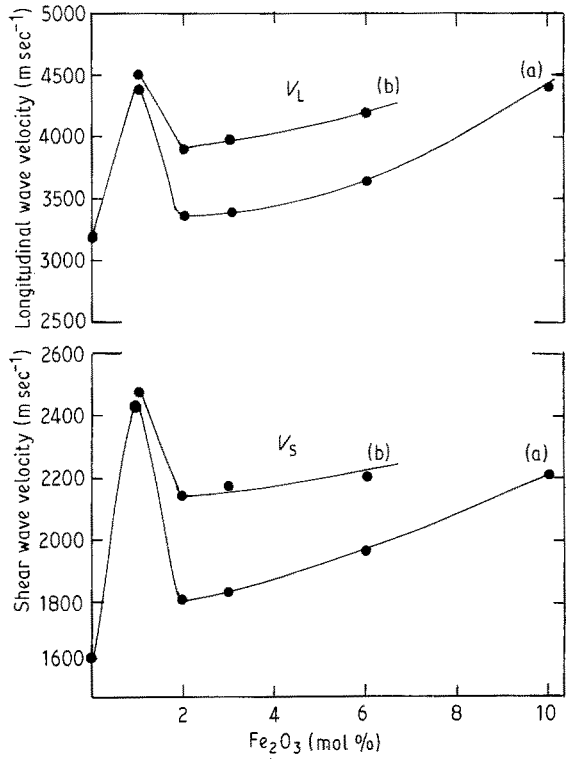

Figure 6 Compositional dependence of longitudinal and shear wave velocities in $(ZrO_2)_{0.9}(Y_2O_3)_{0.1-x}(Fe_2O_3)_x$ ceramic system. (a) and (b) represents specimens fired at 1350 and 1450° C, respectively.

The X-ray diffraction patterns for the $(ZrO_2)_{0.9}(Fe_2O_3)_{0.1}$ specimen are shown in Fig. 4. It can be easily seen that at the firing temperature of 1300° C, both monoclinic and cubic zirconia SS are formed. As the sintering temperature increases, the diffractograms corresponding to monoclinic zirconia grow. This could be correlated with the increased degree of crystallinity as a function of sintering temperature.

3.2. Room temperature elastic constants

Representative data for density, ultrasonic velocities, elastic moduli and Poisson's ratio for the $(ZrO_2)_{0.9}(Y_2O_3)_{0.1-x}(Fe_2O_3)_x$ and $(ZrO_2)_{0.95}(Y_2O_3)_{0.05-x}(Fe_2O_3)_x$ ceramic systems (where X is the compositional mole fraction of Fe_2O_3 content) are plotted as a function of Fe_2O_3 mol % content (see Figs 5–14). The variation of bulk modulus with porosity percentage is shown in Fig. 15.

Recently, polycrystalline elastic moduli data for yttria-stabilized zirconia has been obtained [2, 3, 9, 18, 20] using single crystal elasticity data. The compositional dependence of these elastic moduli data showed an increase with increasing Y_2O_3 mol % content. However, in the present work we try to show the influence of the addition of Fe_2O_3 to Y_2O_3-stabilized ZrO_2 on the elastic constants.

Now, if we first consider the ceramics of composition $(ZrO_2)_{0.9}(Y_2O_3)_{0.1-x}(Fe_2O_3)_x$ fired at 1350° C, the variation of density with Fe_2O_3 mol % (see Fig. 5a) is seen to display an increase up to about 1 mol % Fe_2O_3 content. Beyond 1 mol % the variation of density showed a decrease up to about 10 mol % with a point of inflexion at about 2 mol %. The plot of

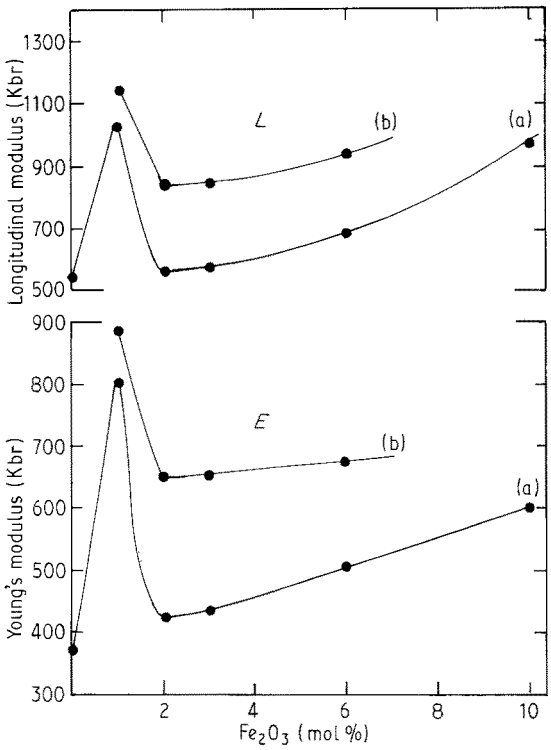

Figure 7 Variation of Young's modulus and longitudinal modulus with Fe_2O_3 mol % for $(ZrO_2)_{0.9}(Y_2O_3)_{0.1-x}(Fe_2O_3)_x$ ceramic system. (a) and (b) denote specimens fired at 1350 and 1450° C, respectively.

density against Fe_2O_3 mol % for specimens fired at 1450° C shows a slight decrease from 0–1 mol % and then behave as the density cure in Fig. 5a (see Fig. 5b). The plots of ultrasonic longitudinal and shear wave velocities against Fe_2O_3 mol % exhibit maxima and minima, respectively, at about 1 and 2 mol % Fe_2O_3 content (see Fig. 6). All the elastic moduli, namely longitudinal, shear, bulk and Young's modulus show

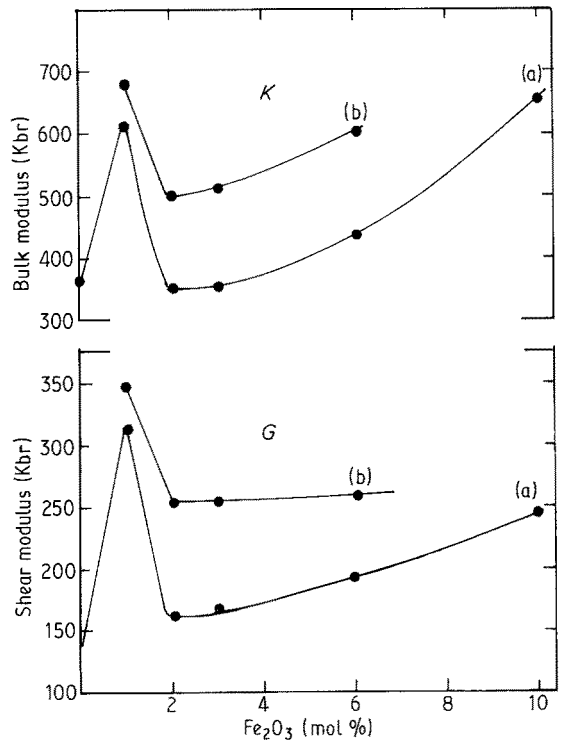

Figure 8 Variation of shear modulus and bulk modulus with Fe_2O_3 mol % for $(ZrO_2)_{0.9}(Y_2O_3)_{0.1-x}(Fe_2O_3)_x$ ceramic system. (a) and (b) denote specimens fired at 1350 and 1450° C, respectively.

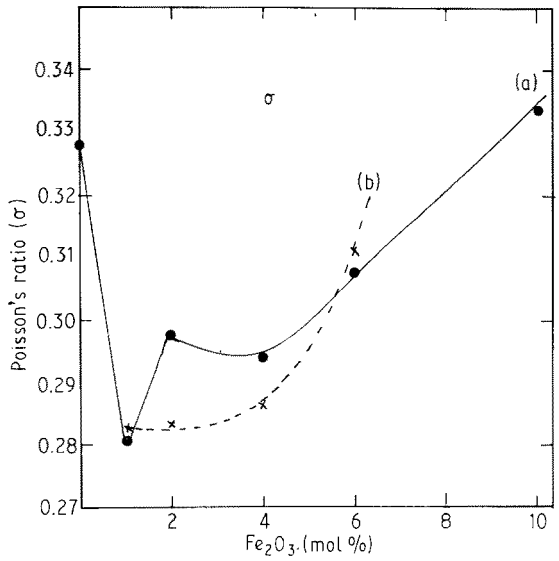

Figure 9 Variation of Poisson's ratio with Fe_2O_3 mol % in $(ZrO_2)_{0.9}(Y_2O_3)_{0.1-x}(Fe_2O_3)_x$ ceramic system. (a) and (b) represents specimens fired at 1350 and 1450° C, respectively.

the same trend as the acoustic wave velocities (see Figs 7 and 8).

Wilhelm *et al.* [13] have reported that the iron dopant can enter the crystal lattice of zirconia ceramic or reside interstatially. In view of the above observation, it seems tempting to suggest that the discontinuities in elastic moduli in our Fe_2O_3 Y_2O_3-stabilized ZrO_2 specimens are to be associated with cations which are able to occupy both interstitial and network forming position. So taking our specific case Fe^{3+} cations enter the network forming positions in the range from 0–1 mol % Fe_2O_3, i.e. the Fe^{3+} substitutes for the Zr^{4+} in the lattice. The effect of the smaller cations (Fe^{3+} 0.069 nm) substituting for the large cation (Zr^{4+} 0.079 nm) causes the lattice spacing to decrease [13]. This led to compact the structure, i.e. introducing the FeO_3 units into the crystal lattice forming positions will cause a decrease in the bonding distances; thus increasing the elastic moduli.

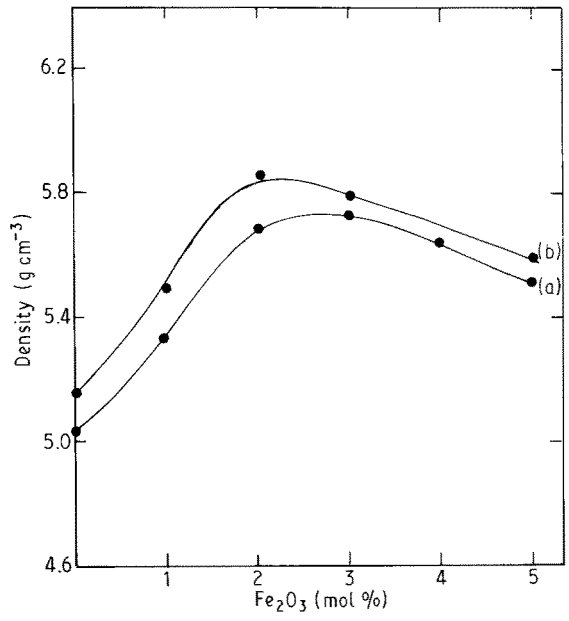

Figure 10 Variation of density with Fe_2O_3 mol % in $(ZrO_2)_{0.95}(Y_2O_3)_{0.05-x}(Fe_2O_3)_x$ ceramic system. (a) and (b) denote specimens fired at 1350 and 1450° C, respectively.

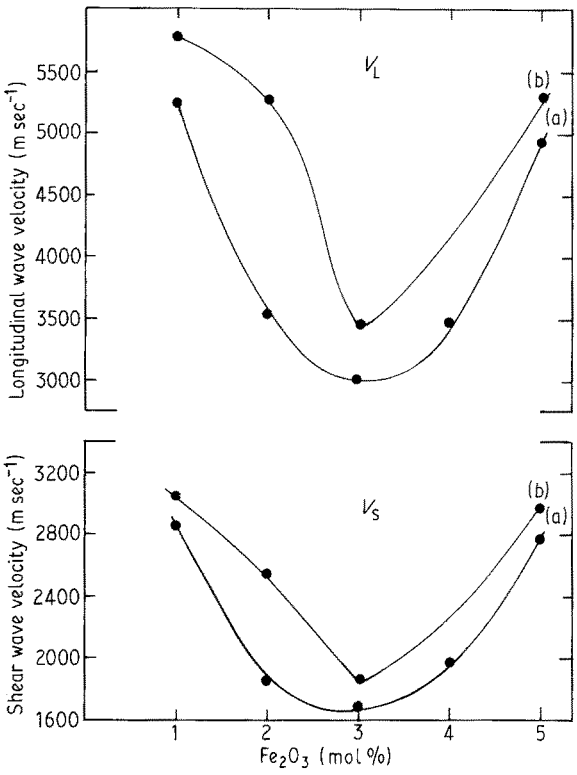

Figure 11 Compositional dependence of longitudinal, and shear wave velocities in $(ZrO_2)_{0.95}(Y_2O_3)_{0.05-X}(Fe_2O_3)_X$ ceramic system. (a) and (b) represents specimens fired at 1350 and 1450° C, respectively.

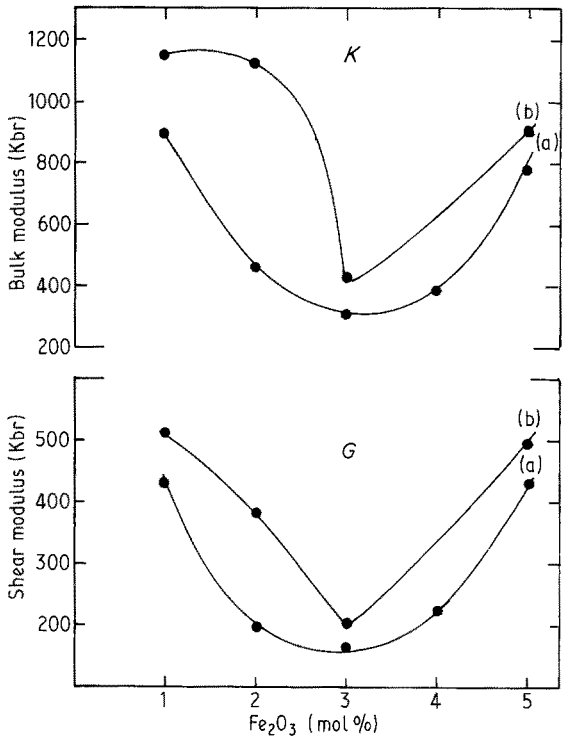

Figure 13 Variation of shear modulus and bulk modulus with Fe_2O_3 mol % in $(ZrO_2)_{0.95}(Y_2O_3)_{0.05-X}(Fe_2O_3)_X$ ceramic system. (a) and (b) denote specimens fired at 1350 and 1450° C, respectively.

In the region 1–2 mol % Fe_2O_3 the elastic moduli decreases, which indicates a structural change in crystal lattice. In this region Fe^{3+} cations may start the enter interstitial positions. This will cause a breaking down of some of the bridging bonds in the network. This alteration in structure will cause an increase in average atomic ring size, thus decreasing the elastic moduli. On the other hand, Lowenstein [24] has claimed that, an atom is assumed generally to possess a higher co-ordination number when sited interstitially. If this assumption was applied to our ceramic, we would conclude that for Fe_2O_3 contents greater than 1 mol % the Fe^{3+} ions entered interstitially with Fe^{3+} cations, fill octahedral vacancies, i.e. they co-ordinate with the six oxygen anions. In octahedral co-ordination the cross-link density of

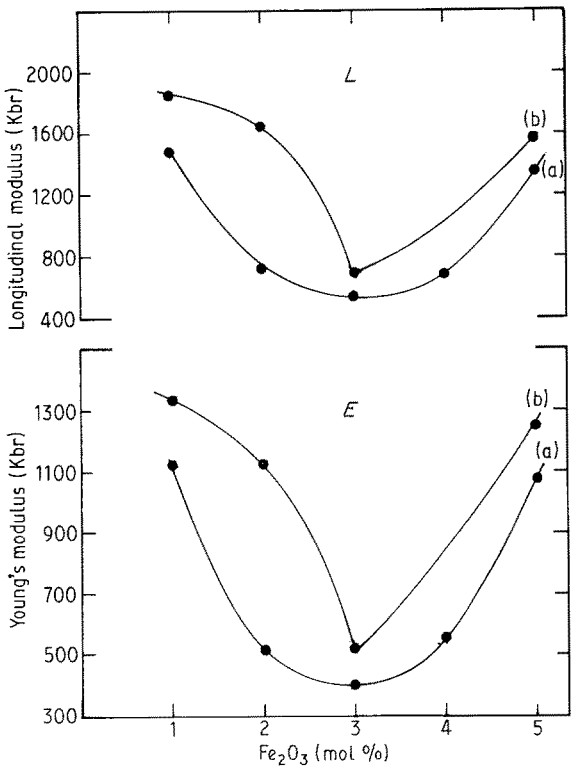

Figure 12 Variation of Young's modulus and longitudinal modulus with Fe_2O_3 mol % for $(ZrO_2)_{0.95}(Y_2O_3)_{0.05-X}(Fe_2O_3)_X$ ceramic system. (a) and (b) denote specimens fired at 1350 and 1450° C, respectively.

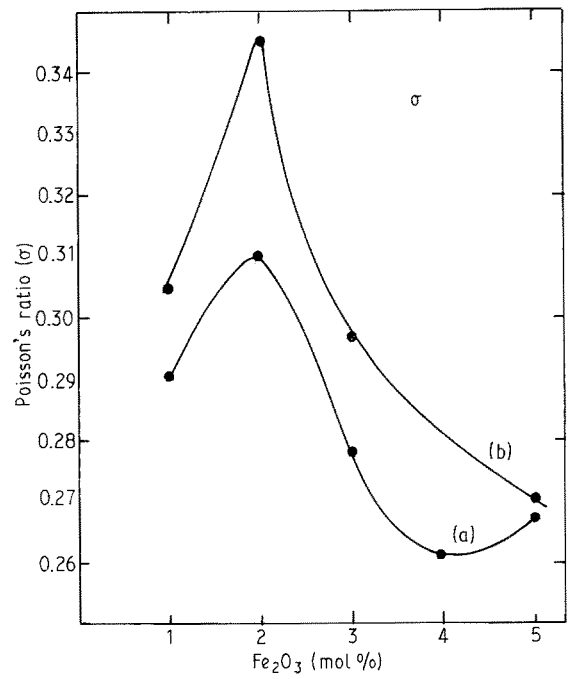

Figure 14 Variation of Poisson's ratio with Fe_2O_3 mol % in $(ZrO_2)_{0.95}(Y_2O_3)_{0.05-X}(Fe_2O_3)_X$ ceramic system. (a) and (b) represents specimens fired at 1350 and 1450° C, respectively.

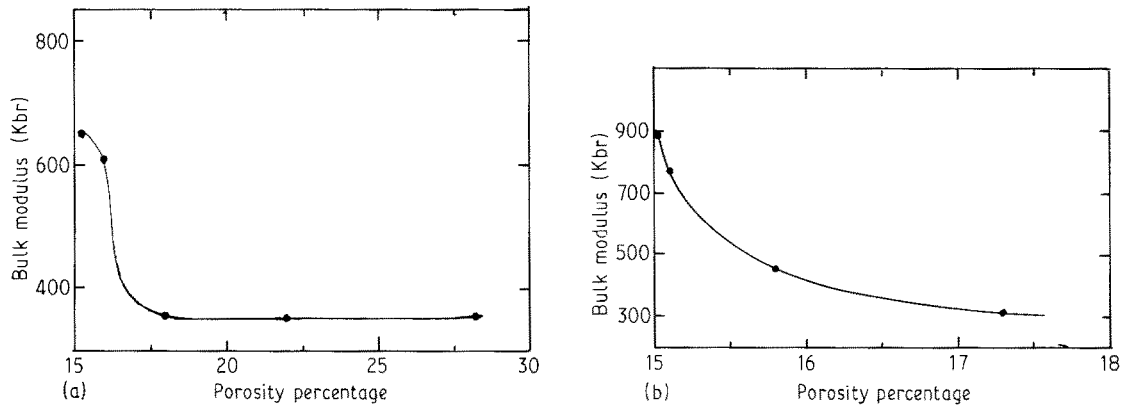

Figure 15 Variation of bulk modulus with porosity percentage in (a) $(ZrO_2)_{0.9}(Y_2O_3)_{0.1-X}(Fe_2O_3)_X$ and (b) $(ZrO_2)_{0.95}(Y_2O_3)_{0.05-X}(Fe_2O_3)_X$ ceramic systems.

Fe^{3+} cation is increased to 4. Therefore, the increasing in elastic moduli with Fe_2O_3 content > 2 mol % can be understood in terms of a gradual transition of Fe^{3+}–O_3 (cross-link density = 1) to Fe^{3+}–O_6 (cross-link density = 4). It appears that when Fe^{3+} ions sited interestitially a mixture of large atomic ring sized (mainly governing the elastic moduli in region 1–2 mol %), and small atomic ring sized (mainly governing the elastic moduli for the compositions > 2 mol %).

Fig. 9 show the plot of Poisson's ratio against mol % Fe_2O_3 content. To interpret our data on the compositional dependence of Poisson's ratio, we gave a qualitative interpretation based on a model put forward by Higazy and Bridge [23], which is summarized as follows:

1. σ decreases with cross-link density (for constant ratio of bond bending to stretching force constant);
2. σ decrease with increasing ratio of bond bending to stretching force constant F_b/F (at constant cross-link density).

Then if these mechanisms are applied in our case,

TABLE I Compositions, densities, longitudinal and shear ultrasonic velocities, elastic moduli and Poisson's ratio for $(ZrO_2)_{1-A}(Y_2O_3)_{A-X}(Fe_2O_3)_X$ specimens fired at 1350° C

Sample no.	ZrO_2 (mol %)	Y_2O_3 (mol %)	Fe_2O_3 (mol %)	Density ϱ (g cm^{-3})	Molar volume (cm^{-3})	Ultrasonic wave velocity (m sec^{-1})		Elastic moduli (Kbr)*				Poisson's ratio σ
						V_L	V_S	Longitudinal L	Shear G	Young's E	Bulk K	
Z-1	90	10	0	5.2872	25.25	3205	1620	543	139	369	358	0.328
Z-2	90	9	1	5.3057	25.03	4398	2430	1026	313	801	609	0.280
Z-3	90	8	2	5.0711	26.06	3345	1794	567	163	423	350	0.298
Z-4	90	7	3	5.0262	26.16	3380	1825	574	167	432	351	0.294
Z-5	90	4	6	5.0110	25.90	3720	1960	693	193	505	436	0.308
Z-6	90	0	10	5.0024	25.36	4418	2208	976	244	651	651	0.334
Z-7	95	5	0	5.0200	25.57	–	–	–	–	–	–	–
Z-8	95	4	1	5.3303	23.96	5248	2849	1468	433	1118	891	0.291
Z-9	95	3	2	5.6870	22.34	3531	1852	709	195	511	449	0.310
Z-10	95	2	3	5.7175	22.10	3011	1670	518	159	406	306	0.278
Z-11	95	1	4	5.6398	22.31	3475	1975	681	220	555	388	0.261
Z-12	95	0	5	5.5051	22.71	4926	2777	1336	425	1077	769	0.267

*1 Kbr = 10^9 dym/cm^2

TABLE II Compositions, densities, longitudinal and shear ultrasonic velocities, elastic moduli and Poisson's ratio for $(ZrO_2)_{1-A}(Y_2O_3)_{A-X}(Fe_2O_3)_X$ specimens fired at 1450° C

Sample no.	ZrO_2 (mol %)	Y_2O_3 (mol %)	Fe_2O_3 (mol %)	Density ϱ (g cm^{-3})	Molar volume (cm^{-3})	Ultrasonic wave velocity (m sec^{-1})		Elastic moduli (Kbr)*				Poisson's ratio σ
						V_L	V_S	Longitudinal L	Shear G	Young's E	Bulk K	
Z-1	90	10	0	5.6601	23.58	–	–	–	–	–	–	–
Z-2	90	9	1	5.6474	23.52	4502	2481	1145	348	892	681	0.282
Z-3	90	8	2	5.5385	23.86	3891	2142	838	254	652	499	0.283
Z-4	90	7	3	5.3700	24.49	3975	2175	848	254	653	409	0.286
Z-5	90	4	6	5.3109	24.44	4210	2203	941	258	676	597	0.311
Z-6	90	0	10	5.3060	23.91	–	–	–	–	–	–	–
Z-7	95	5	0	5.1470	24.94	–	–	–	–	–	–	–
Z-8	95	4	1	5.4875	23.27	5763	3052	1823	511	1334	1142	0.305
Z-9	95	3	2	5.8622	21.67	5267	2550	1626	381	1025	1118	0.345
Z-10	95	2	3	5.7870	21.84	3459	1859	692	200	519	425	0.297
Z-12	95	0	5	5.5905	22.37	5275	2961	1556	490	1245	903	0.270

*1 Kbr = 10^9 dym/cm^2

we find that the variation of Poisson's ratio with composition ought to be exactly the reverse of the elastic moduli variation. From inspection the variation of Poisson's ratio composition (Fig. 9) one can find that σ behaves as proposed in the compositional region 1–2 mol %. However, in the region 2–10 mol %, σ showed a slight increase. In fact we have no explanation of this notion at the present time.

For, the $(ZrO_2)_{0.95}(Y_2O_3)_{0.05-X}(Fe_2O_3)_X$ ceramic system we have identified two composition regions from the compositional dependence of the density, the elastic moduli and Poisson's ratio (see Figs 10–14). To interpret these results the same explanation which has been applied to the composition regions 1–2 and 2–10 mol % in the previous $(ZrO_2)_{0.9}(Y_2O_3)_{0.1-X}(Fe_2O_3)_X$ system, can be used to explain the compositional dependence in the composition regions 1–3 and 3–5 mol %, respectively. However, from inspection of the compositional dependence of the density, ultrasonic wave velocities and the elastic moduli data shown in Figs 10–13, we note that, these data showed higher values than those has been obtained for the previous $(ZrO_2)_{0.9}(Y_2O_3)_{0.1-X}(Fe_2O_3)_X$ ceramic system (see Figs 5–8). Also, all the data for specimens fired at 1450° C showed higher values than those specimens fired at 1350° C (Tables I and II).

Figures 15a and b show the bulk modulus as a function of porosity. It was observed that the elastic moduli decreases with increasing the porosity percentage for our ceramic samples.

References

1. C. F. SMITH and W. B. CRANDALL, *J. Amer. Ceram. Soc.* **47** (12) (1964) 624.
2. N. G. PACE, G. A. SAUNDERS, Z. SUMENGEN and J. S. THORP, *J. Mater. Sci.* **4** (1969) 1106.
3. G. SIMMONS and H. WANG, "Single Crystal Elastic Constants and Calculated Aggregate Properties A Handbook", (MIT Press, Cambridge, MA, 1971).
4. J. M. FARLEY, J. S. THORP, J. S. ROSS and G. A. SAUNDERS, *J. Mater. Sci. Lett.* **7** (1972) 475.
5. W. J. FLEMING, D. S. HOWARTH and D. S. EDDY, *SAE Tran.* **82** (1973) 1969.
6. V. I. ALEKSANDROV, V. F. KITAEVA, I. V. KOZLOV, V. V. OSIKO, N. N. SOBLOEV, V. M. TATARINTSEV and I. L. CHISTYI, *Sov. Phys. Crystallogr.* **18** (5) (1974) 682.
7. V. I. ALEKSANDROV, V. F. KITAEVA, V. V. OSIKO, N. N. SOBOLEV, V. M. TATRINTSEV and I. L. CHISTYI, *Kratkie Soobshchentya Po Fizike* **3** (1975) 21.
8. H. DUEKER, K. H. FRIESE and W. D. HAECKER, *ibid.* **84** (1975) 807.
9. V. I. ALEKSANDROV, V. F. KITAEVA, I. V. KOZLOV, V. V. OSIKO, N. N. SOBLOEV, V. M. TATARINTSEV and I. L. CHISTYI, *Sov. Phys. Solid State* **16** (8) (1975) 1456.
10. I. L. CHISTYI, I. L. FABELINSKII, V. F. KITAEVA, V. V. OSIKO, YU. V. PISALEVSKII, I. M. SILL'VESTROVA and N. N. SOHOLEV, *J. Raman Spectroscopy* **6** (4) (1977) 183.
11. E. HAMANN, H. MANGER and L. STEINKE, "Lambda-Sensor with Y_2O_3-stabilized ZrO_2-ceramic for Application in Automotive Emission Control System", in "Automotive Applications of Sensors", Special Publication No. 418, (Society of Automotive Engineers, Warrendale, PA, 1977) p. 53–58.
12. S. L. DOLE, O. HUNTER, Jr and C. J. WOOGE, *J. Amer. Ceram. Soc.* **60** (11, 12) (1977) 488.
13. R. V. WILHELM, J. R. and D. S. HOWARTH, *Ceram. Bulletin* **58** (2) (1979) 228.
14. O. HUNTER, Jr, R. W. SCHEIDECKER and SETSUO TOJO, *Ceram. Inter.* **5** (4) (1979) 137.
15. S. L. DOLE, O. HUNTER, Jr and F. W. CALDERWOOD, *J. Amer. Ceram. Soc.* **63** (3, 4) (1980) 136.
16. A. H. HEUER and L. W. HOBBS (eds), "Science and Technology of Zirconia-Advances in Ceramics", Vol. 3, (American Ceramics Society, Chicago, 1981).
17. K. JYECHEN and Y. CHAOKO, *Ceram. Bulletin* **62** (9) (1983) 1030.
18. A. J. A. WINNUBST, K. KEIZER and A. J. BURGGRAAF, *J. Mater. Sci.* **18** (1983) 1958.
19. N. CLAUSSEN, M. RUHLE and A. H. HEUER (eds), "Science and Technology of Zirconia-Advances in Ceramics, Vol. 12, (American Ceramic Society, San Francisco, 1984).
20. H. M. KANDIL, J. D. GREINER and J. F. SMITH, *J. Amer. Ceram. Soc.* **67** (5) (1984) 341.
21. R. P. INGEL, D. LEWIS, B. A. BENDER and R. W. RICE, "Advances in Ceramics" Vol. 12, edited by N. Claussen, M. Ruhle and A. H. Heuer (American Ceramic Society, 1984) pp. 408–14.
22. M. A. EWAIDA, E. M. H. IBRAHIM, M. M. ABOU SEKKINA and A. A. AL-ADAWY, XXV Colloquium Spectroscopieum International Conference, Toronto, Canada, 6 June (1987), in press.
23. A. A. HIGAZY and B. BRIDGE, *J. Non-Crystall. Solids* **72** (1985) 81.
24. K. L. LOWENSTEIN, *Phys. Chem. Glasses* **2** (1961) 69.

Received 30 June
and accepted 18 November 1988